RSC Advances

PAPER

View Article Online
View Journal | View Issue

Cite this: *RSC Adv.*, 2023, **13**, 28686

Facile synthesis of a new covalent organic nanosheet (CON-KEY1) based on polyamide links as an effective heterogeneous catalyst in C–C cross coupling reactions

Hassan Keypour, *[a] Jamal Kouhdareh,[a] Rahman Karimi-Nami,[b] Idris Karakaya,[c] Molood Abdollahi-Moghadam,[a] Khadijeh Rabiei[d] and Sedigheh Alavinia[a]

C–C coupling reactions represent a fundamental synthetic methodology widely employed in academic and industrial settings. Herein, we present a report on developing and synthesizing a heterogeneous catalyst that is environmentally compatible and has recycling capabilities. Furthermore, the utilization of this catalyst for C–C coupling reactions was explored. A novel amide-based CON was prepared *via* the reaction of a novel [2,2′-bipyridine]-5,5′-diamine (BDA) and 1,3,5-tris(4-carboxyphenyl) (TCB). TCB was activated with carbonyl diimidazole (CDI) and then reacted with BDA to synthesize favorable CON (*i.e.*, CON-KEY1). Finally, the CON synthesized was reacted with palladium chloride ions, and the palladium-containing organocatalytic complex was decorated with the abbreviated Pd/CON-KEY1. This new heterogeneous complex was fully characterized through the required techniques, including FT-IR, EDX, XRD, TEM, SEM, ICP, TGA-DTA, N_2 isotherms, and elemental mapping analysis. Computer simulation results include a multi-sheet 2D framework proposed by CON-KEY1. As a result, palladium ions were found to be arranged between the layers and on the CON surface. This heterogeneous complex functioned as a catalyst precursor in both the Suzuki–Miyaura coupling reaction of aryl boronic acids with aryl halides and the Heck reaction of aryl halides with acrylate derivatives or styrene. The desired coupling products with various functional groups were successfully attained with excellent yields of up to 98%. Simple set-up, improved yields, short reaction times, non-toxic solvents, catalyst durability, and high turnover frequency are among the distinct advantages of this synthetic method. Some other outstanding features of this catalytic system include convenient separation of catalysts and products, high yields, almost complete conversion, high selectivity, and good turnover frequency (TOF). The results show that the highest product efficiency in the reaction was achieved in the shortest possible time using Pd/CON-KEY1. Theoretical studies demonstrated the precedence of the palladium complexation with nitrogen atoms of CON-KEY1 rather than oxygen ones. Natural Bond Orbital (NBO) analysis affirmed that the system with Pd–N bonds (E_g = 0.089 eV) is more reactive with high electron conductivity compared to the Pd–O system (E_g = 0.120 eV).

Received 19th August 2023
Accepted 23rd September 2023

DOI: 10.1039/d3ra05664c

rsc.li/rsc-advances

1. Introduction

Covalent organic frameworks (COFs) and Covalent Organic Nanosheets (CONs) are emerging types of organic polymers, with permanent porosity and highly ordered structures, which are two- or three-dimensional (2D or 3D) porous crystalline structures prepared through reticular chemistry. In contrast to other polymers, a key feature of COFs and CONs is that they are structurally predesignable, synthetically controllable, and functionally manipulable. Indeed, topological design diagrams provide a geometric guide for structural tiling of extended porous polygons, and polycondensation reactions guide synthetic routes for building predesigned primary and higher-order structures.[1–8]

Due to their extraordinary properties in structural engineering and ordered structures, CONs are good candidates for acting as ligands, forming metal complexes, and depositing metal nanoparticles on substrates.[9] In fact, due to nitrogen groups in the bonds between structures, CONs may form complexes that can be used as excellent supports in catalysis-related reactions.[2,10–13] Moreover, a critical point in using

[a]*Faculty of Chemistry, Bu-Ali Sina University, Hamedan 65174, Iran. E-mail: haskey1@yahoo.com*
[b]*Department of Chemistry, Faculty of Science, University of Maragheh, Maragheh, Iran*
[c]*Department of Chemistry, College of Basic Sciences, Gebze Technical University, 41400 Gebze, Turkey*
[d]*Department of Chemistry, Faculty of Science, Qom University of Technology, Qom, Iran*

Table 1 Mizoroki–Heck cross-coupling reactions in the pharmaceutical industry

Structure	Company	Usage	Scale	Catalyst/reaction conditions	Reference
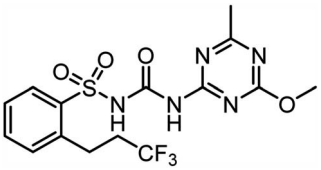	Novartis	Herbicide	Multi – ton	$Pd(dba)_2$ 25 °C ton 200; TOF *ca.* 50 h^{-1}	24 and 25
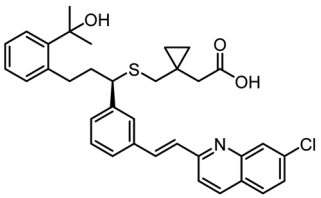	Merck	Asthma drug	—	$Pd(OAC)_2$ Et_2N, MeCN 85 °C	26
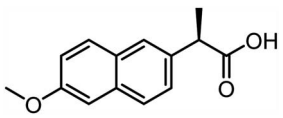	Albermarle, Hoechst AG	Non-steroidal antiinflammatory drug	Multi – ton	$PdCl_2$, $CuCl_2$	24 and 27–29
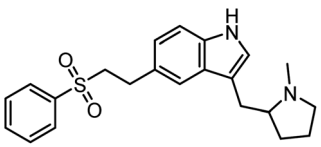	Pfizer	Migraines	Multi-kg	$Pd(OAC)_2$/P(*o*-tolyl)$_3$ Et_3N, DMF, reflux 80% yield	30
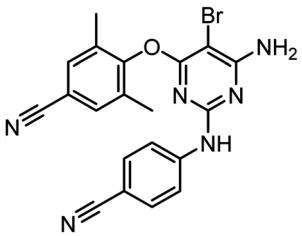	Johnson & Johnson	HIV	6k L	$Pd(OAc)_2$/tri-*o*-toly-phosphine	25–31
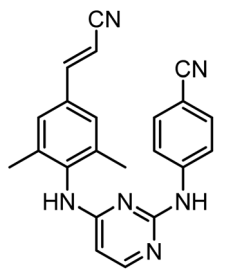	Johnson & Johnson	HIV	6k L	$Pd(OAc)_2$, P(*o*-tol)$_3$, Et_3N, CH_3CN, 150 °C	26–31
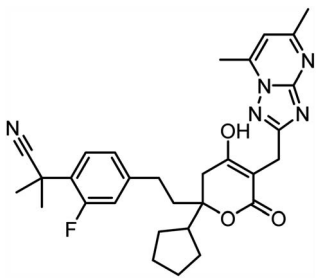	Pfizer	Hepatitis C polymerase inhibitor	40 kg scale	$Pd(OAC)_2$ LiCl LiOAc Et_3N	32

covalent organic frameworks as supports for heterogeneous catalytic systems is their high specific surface area and facile separation from the reaction mixture.[12,14]

Our aim for using CONs as catalyst supports is that it provides a unique basis for using these mesoporous polymers in catalysis. A cross-coupling reaction is a transformation in which two fragments are joined together with the help of a metal catalyst. One of the most important reasons for using palladium-containing catalysts is their ability to perform carbon–carbon and carbon–nitrogen cross-coupling reactions.[15–20]

Biaryls and cinnamic acid derivatives are two classes of organic compounds synthesized by two-component condensation reactions, such as cross-coupling. These units are increasingly important in organic chemistry due to their presence in the structures of various natural products and bioactive compounds.[2,21,22] As a result, several studies have been carried out on synthesizing various organic materials containing these moieties using the Suzuki and Heck reactions. Due to the application of different heterogeneous and homogeneous catalysts, bioactivity, and structural properties of Suzuki and Heck coupling compounds, several specific processes have been developed (Table 1).[23–25]

Despite reported synthetic methods for these catalysts, it is believed that much research is still needed in this area. Therefore, there is a need to develop additional environmentally friendly, atomically efficient, sustainable, and high-yielding methods.

In this study, a novel two-dimensional Covalent Organic Nanosheet (CON-KEY1) based on synthetic polyamide compounds was designed and fabricated. A carbonyldiimidazole (CDI) activator compound activated the carboxylic acid groups. In the next step, we synthesized a new CON-KEY1 and then used it to support preparing organopalladium nanocatalysts. In this paper, we report the preparation of new CON-KEY1 based on polyamide links as an effective heterogeneous catalyst for Suzuki–Miyaura coupling reaction of aryl boronic acids with aryl halides and Heck reaction of aryl halides

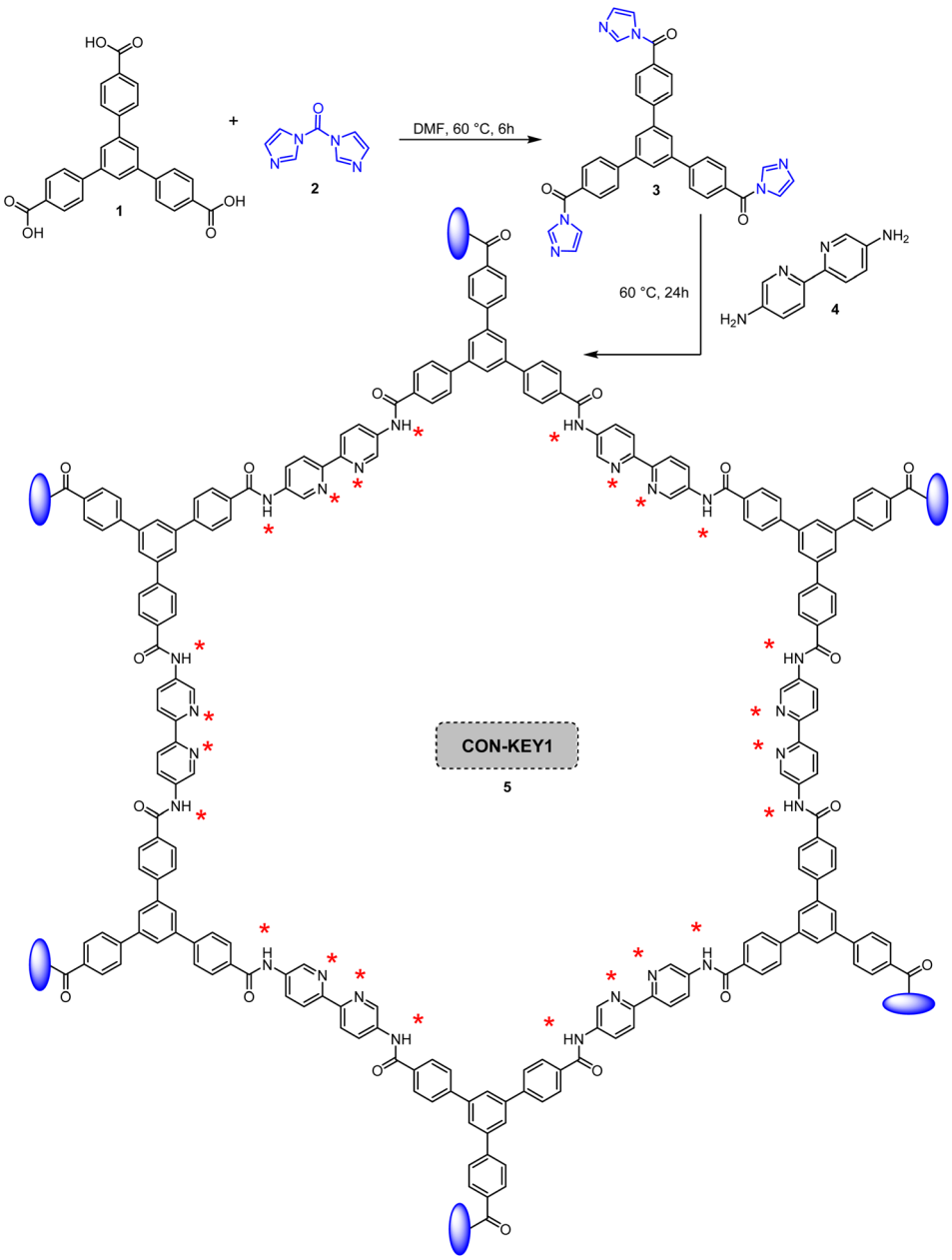

Scheme 1 Preparation of CON-KEY1 **5**.

with acrylate derivatives or styrene and excellent results have been obtained with high efficiency.

2. Experimental

2.1. Synthesis of CON-KEY1 (5)

COF-KEY1 **5** was synthesized by reacting CDI **2**, [2,2′-bipyridine]-5,5′-diamine (BDA) **4** and 1,3,5-tris(4-carboxyphenyl)benzene **1** (TCB). For this purpose, TCB **1** (29.0 mmol) and CDI **2** (30.0 mmol) were dissolved in DMF (50 mL) and sonicated for 30 min. The reaction was then shaken at 60 °C for 6 h. BDA **4** was then added and shaken for 24 h. The solid that formed was filtered and washed with dichloromethane. The CON **5** thus produced was then placed in dichloromethane (25 mL), and the DMF was removed for 24 h. Finally, the prepared CON **5** was rinsed with dichloromethane and dried in an oven at 50 °C for 6 h (Scheme 1).[26]

2.2. Preparation of Pd/CON-KEY1 6

2.0 g of CON-KEY1 **5** was poured into a beaker, and 60 mL of acetonitrile was added and sonicated for 1 h until wholly dispersed. 50 mg of the palladium chloride salt was then dispersed in 10 mL of acetonitrile and added to the nanoparticles **5** dispersion, and the reaction mixture was refluxed at 50 °C for 24 h. Finally, the Pd/CON-KEY1 **6** was separated by centrifugation, washed with ethanol, and dried in an oven at 50 °C for 12 h. The Pd loading of the material was estimated to be 3.14 mmol g^{-1} by the ICP-OES technique (Scheme 2).

2.3. General procedure for the Mizoroki–Heck reaction

An oven-dried 25 mL round bottom flask with a magnetic stirrer bar was charged Pd/CON-KEY1 **6** (30 mg) in DMF (5 mL). The reaction mixture was stirred for 3 min under argon. To this reaction mixture, base K_2CO_3 (2 mmol), aryl iodide (1 mmol), olefin (1–2.5 mmol), and DMF (5 mL) were added, and the reaction mixture was stirred at the indicated temperature and time. TLC monitored the reaction. The reaction mixture was quenched with water (10 mL) and extracted with ethyl acetate (10 mL). The organic layer was washed with brine, dried over Na_2SO_4, and concentrated under vacuum. The residue was purified by column chromatography on silica gel to give the desired product.

2.4. General procedure for the catalysis of the Suzuki–Miyaura coupling

To a solution of aryl halide (0.078 g, 0.5 mmol), aryl boronic acid (0.073 g, 0.6 mmol), K_3PO_4 (0.127 g, 0.6 mmol) in DMF or dioxane and water (1 : 1, 10 mL), was added Pd/CON-KEY1 **6** (50 mg). The resulting mixture was heated by stirring at 100 °C under argon for 2–6 h. The reaction mixture was quenched by adding water and extracted with ethyl acetate (3 × 20 mL). The combined extract was washed with saturated brine and dried over anhydrous Na_2SO_4. The organic layer was concentrated under vacuum, and the crude product was purified by column chromatography on silica gel (100–200 mesh, petroleum ether: 2% ethyl acetate) to give the pure desired product.

2.5. Spectral information of some reaction products

2.5.1 2-Propenoic acid-3-phenyl, ethyl ester. Obtained as a colorless oil, ^{1}H NMR (400 MHz, $CDCl_3$, δ): 7.65–7.73 (d, J = 16 Hz, 1H), 7.33–7.58 (m, 5H), 6.45 (d, J = 16 Hz, 1H), 4.23 (q, J = 7.2 Hz, 2H), 1.33 (t, J = 7.1 Hz, 3H); ^{13}C NMR (100 MHz, $CDCl_3$, δ): 168.3, 146.5, 135.3, 131.3, 126.8, 127.7, 119.2, 61.5, 15.2.

2.5.2 (*E*)-1,2-Diphenylethene. Obtained as a white solid, mp: 123.5–124.5 °C, ^{1}H NMR (400 MHz, $CDCl_3$, δ) 7.55–7.3 (m, 10H), 7.13 (s, 2H); ^{13}C NMR (100 MHz, $CDCl_3$, δ) 138.3, 129.7, 127.5, 126.5.

2.5.3 Ethyl (*E*)-3-(4-methoxyphenyl)acrylate. Obtained as a colorless oil, ^{1}H NMR (400 MHz, $CDCl_3$, δ) 7.63 (d, J = 15.9 Hz, 1H), 7.47 (d, J = 8.7 Hz, 2H), 6.89 (d, J = 8.9 Hz, 2H), 6.30 (d, J = 16 Hz, 1H), 4.25 (q, J = 7 Hz, 2H), 3.83 (s, 3H), 1.31 (t, J = 7.2 Hz, 3H); ^{13}C NMR (100 MHz, $CDCl_3$, δ) 167.33, 161.3, 144.2, 129.6, 127.1, 115.7, 114.3, 60.3, 55.32, 14.3.

2.5.4 (*E*)-1-Methoxy-4-styrylbenzene. Obtained as a white solid, mp: 135–136 °C, ^{1}H NMR (400 MHz, $CDCl_3$, δ) 7.53–7.24 (m, 7H), 7.04 (d, J = 7.45 Hz, 2H), 6.91 (d, J = 8.45 Hz, 2H), 6.32 (d, J = 16 Hz, 1H), 4.25 (q, J = 7.2 Hz, 2H), 3.85 (s, 3H), 1.33 (t, J = 7.2 Hz, 3H); ^{13}C NMR (100 MHz, $CDCl_3$, δ) 158.3, 138.2, 131.1, 129.1, 128.1, 127.7, 127.1, 126.5, 126.3, 114.1, 55.3.

2.5.5 2-Propenoic acid, 3-(4-methyl phenyl)-ethyl ester. Obtained as a colorless oil, ^{1}H NMR (400 MHz, $CDCl_3$, δ): 7.55 (d, J = 16.0 Hz, 1H), 7.33 (d, J = 8.0 Hz, 2H), 7.08 (d, J = 7.8 Hz, 2H), 6.30 (d, J = 15.9 Hz, 1H), 4.14 (q, J = 7.1 Hz, 2H), 2.27 (s, 3H), 1.25 (t, J = 7.1 Hz, 3H); ^{13}C NMR (100 MHz, $CDCl_3$, δ): 168.1, 145.4, 141.3, 130.9, 129.5, 128.1, 118.3, 76.7, 76.5, 61.5, 21.5, 14.5.

2.5.6 2-Propenoic acid, 3-(4-fluorophenyl)-ethyl ester. Obtained as a colorless oil, ^{1}H NMR (400 MHz, $CDCl_3$, δ) 7.65 (d, J = 16 Hz, 1H), 7.55–7.46 (m, 2H), 7.30–7.05 (m, 2H), 6.37 (d, J = 16.17 Hz, 1H), 4.27 (q, J = 7.20 Hz, 2H), 4.10 (q, J = 7.07 Hz, 2H, E : Z ratio 8.6 : 1), 1.34 (t, J = 7.07 Hz, 3H), 1.15 (t, J = 7.2 Hz, 3H, E : Z ratio 8.8 : 1); ^{13}C NMR (100 MHz, $CDCl_3$, δ) 167.7, 167.2–162.3 (d, J_{C-F} = 252.6 Hz), 144.1, 132.1, 131.0, 130.5, 129.7, 129.5, 118.7, 116.1, 115.5, 115.3, 114.6, 60.2, 60.0, 15.1, 13.9.

2.5.7 4-Chloro-1,1′-biphenyl. Obtained as a white solid, mp: 77–78.5 °C, ^{1}H NMR (400 MHz, $CDCl_3$, δ) −7.61–7.38 (m, 9H); ^{13}C NMR (100 MHz, $CDCl_3$, δ) – 140.0, 139.7, 134.3, 129.7, 128.3, 126.8.

2.5.8 1,1-Biphenyl. Obtained as a white solid, mp: 67–68 °C, ^{1}H NMR (200 MHz, $CDCl_3$, δ) 7.62–7.56 (m, 4H), 7.49–7.3 (m, 6H).

2.5.9 4-Chloro-4-methyl-1,1-biphenyl. Obtained as a white solid, mp: 121–123 °C, ^{1}H NMR (400 MHz, $CDCl_3$, δ) 7.55–7.43 (m, 6H), 7.25–7.24 (m, 2H), 2.44 (s, 3H); ^{13}C NMR (100 MHz, $CDCl_3$, δ) 144.1, 142.5, 141.3, 138.4, 131.5, 129.8, 128.4, 128.1, 127.7, 127.5, 127.4, 127.3, 126.6, 115.5, 87.5, 83.3, 68.9, 65.2, 64.3.

2.5.10 1-(4-Methoxyphenyl)-naphthalene. Obtained as a white solid, mp: 114–115 °C, ^{1}H NMR (400 MHz, $CDCl_3$, δ) 7.95–7.83 (m, 3H), 7.55–7.42 (m, 6H), 7.06–7.02 (d, J = 8.84 Hz, 2H), 3.93 (s, 3H); ^{13}C NMR (100 MHz, $CDCl_3$, δ) 132.1, 128.3, 127.4, 126.8, 126.1, 125.6, 125.87 125.4, 114.1, 55.2.

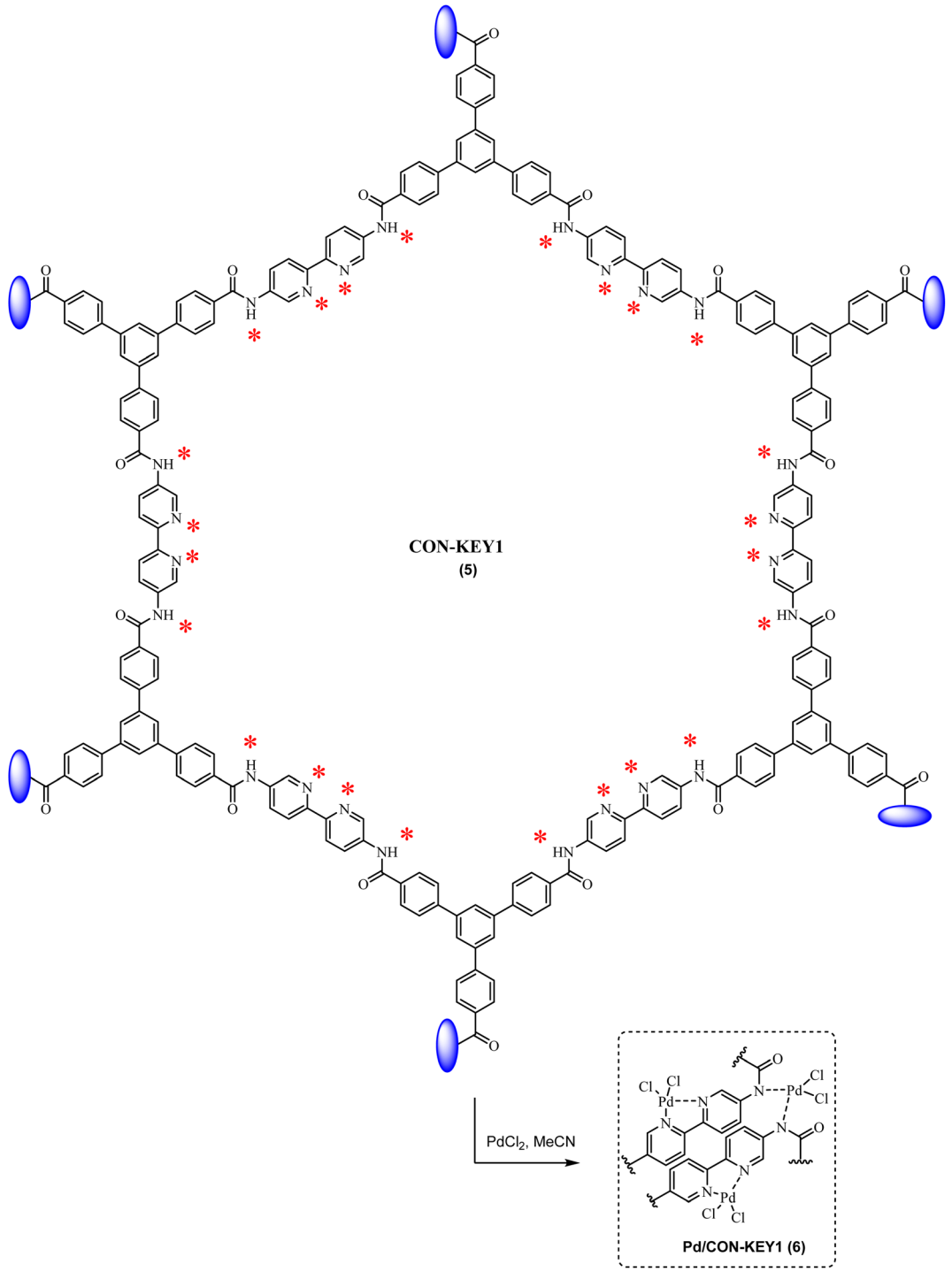

Scheme 2 Preparation of Pd/CON-KEY1 **6**.

2.5.11 4-Methoxy-1,1-biphenyl. Obtained as a white solid, mp: 89–91 °C, ^{1}H NMR (400 MHz, $CDCl_3$, δ) 7.58–7.51 (m, 4H), 7.48–7.32 (m, 3H), 7.00 (d, J = 8.84 Hz, 2H), 3.87 (s, 3H); ^{13}C NMR (100 MHz, $CDCl_3$, δ) 129.1, 128.1, 126.7, 126.3, 112.2, 55.3.

2.5.12 4-Methyl-1,1′-biphenyl. Obtained as a white solid, mp:−49 °C, ^{1}H NMR (400 MHz, $CDCl_3$, δ): 7.17–7.63 (m, 9H), 2.39 (s, 3H).

2.6. Computational details

The structures of CON-KEY1 **5**, Pd–N/CON-KEY1 **6**, and Pd–O/CON-KEY1 **6** were investigated by DFT calculations using Gaussian16 at B3LYP/lanl2dz level of theory, and initial optimizations were performed by HyperChem 8. Besides, the optimized structures binding energies, bond lengths, and bond angles were evaluated while not displaying any imaginary

frequency. NBO analyses were done to indicate the frontier orbitals, band gaps, HOMO–LUMO representations, and the global descriptors.

3. Result and discussion

3.1. Catalyst characterization

Fig. 1 illustrates the Fourier transform infrared (FT-IR) spectra of CON-KEY1 **5** and Pd/CON-KEY1 **6** nanocomposites. Fig. 1 – blue displays the CON-KEY1s **5** characteristic IR peaks at 1654 and 3420 cm^{-1}, attributed to C=O and N–H stretching, respectively. These peaks prove the establishment of the amide-based CON (Fig. 1-blue). The FT-IR spectrum of the synthesized catalyst shows a peak shift in the region of 1654 to 1668 cm^{-1}, which is due to the binding of palladium metal and the formation of an organopalladium complex with a nanocomposite structure[27–30] (Fig. 1-orange).

Fig. 2 illustrates the TGA of the prepared CON-KEY1 **5** (A) and Pd/CON-KEY1 **6** (B). Fig. 2 shows considerable weight loss occurs at 130–250 °C for CON-KEY1 **5** (thermogram A) and Pd/CON-KEY1 **6** (thermogram B). This weight loss is attributed to the loss of organic moieties. The weight loss observed at a temperature of less than 250 °C is related to the evaporation of the trapped solvents in the synthesized nanocomposite structure. The decreasing slope in the 250 to 420 °C temperature range is due to removing functional groups in the corresponding nanocomposite structure. These results mean high thermal stability for this nanocatalyst and show the usefulness of using these structures as metal ions support.

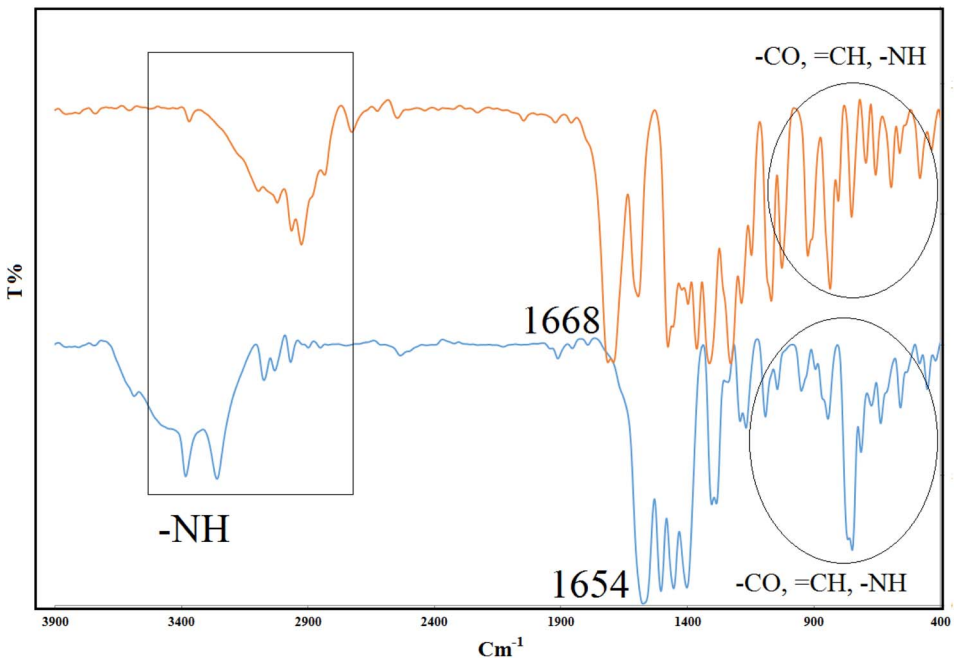

Fig. 1 FT-IR spectrum of (blue) CON-KEY1 **5**, (orange) Pd/CON-KEY1 **6**.

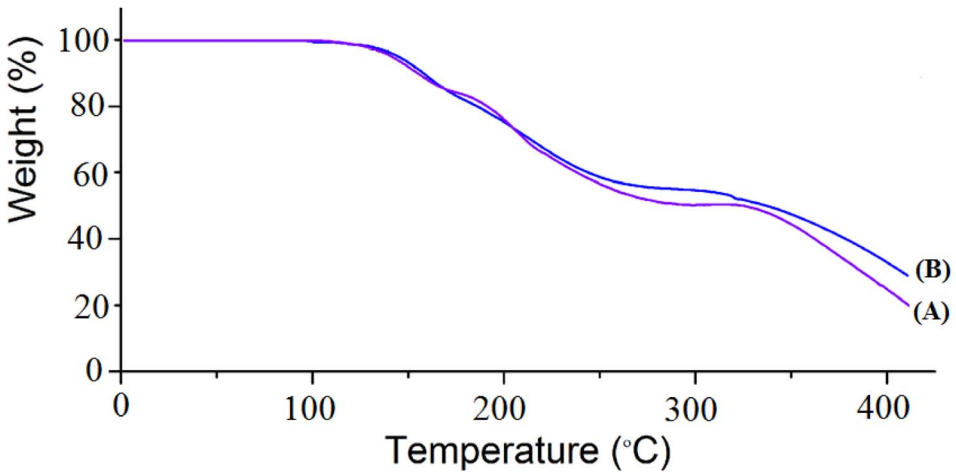

Fig. 2 TGA plots of the (A) CON-KEY1 **5** and (B) Pd/CON-KEY1 **6**.

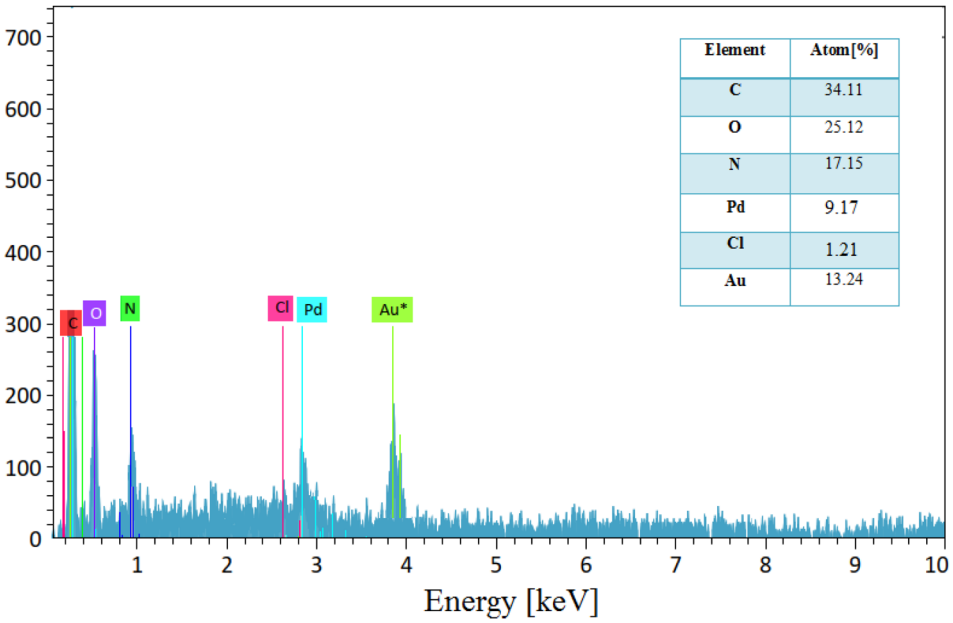

Fig. 3 EDX spectrum of Pd/CON-KEY1 **6**.

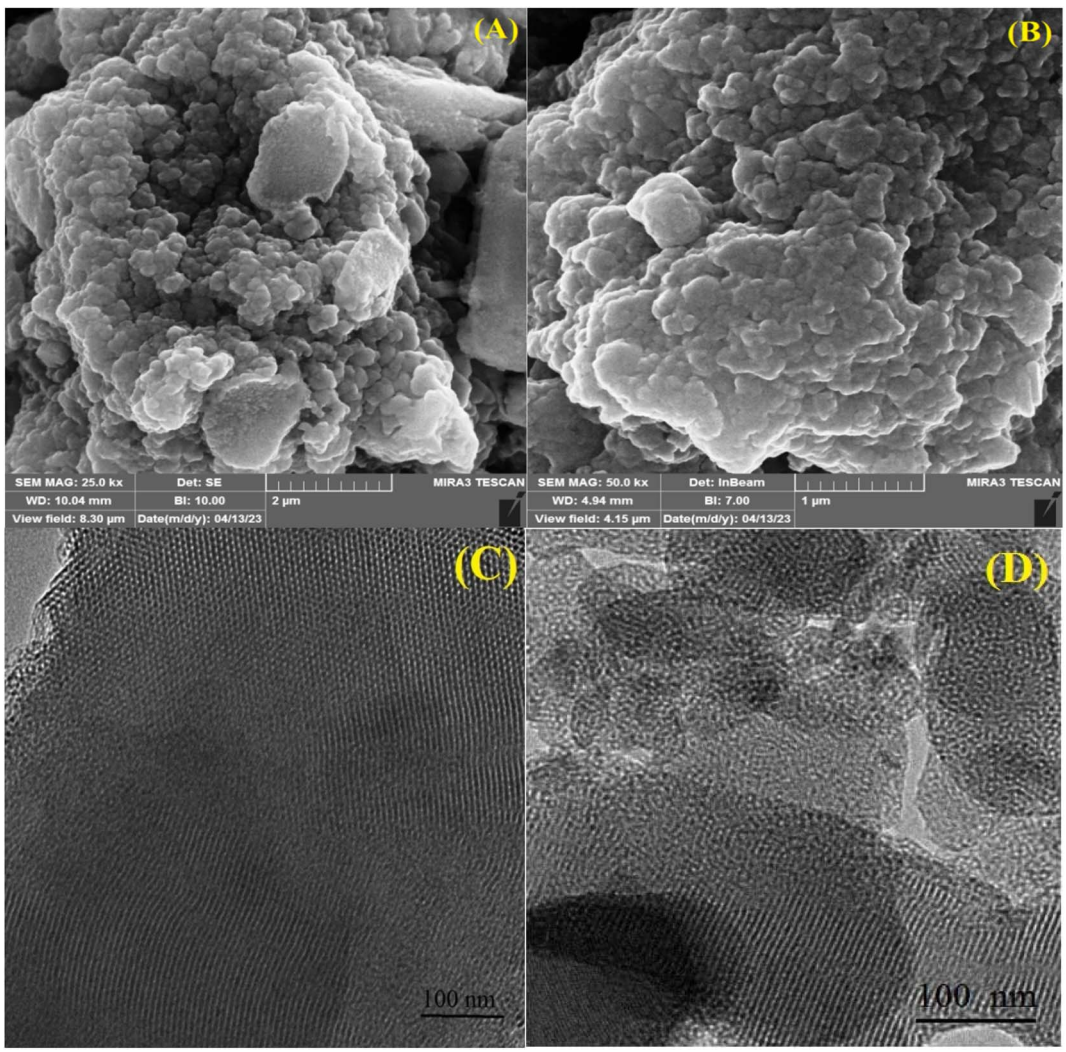

Fig. 4 SEM images of (A and B) Pd/CON-KEY1 **6**, and (C and D) TEM images of Pd/CON-KEY1 **6**.

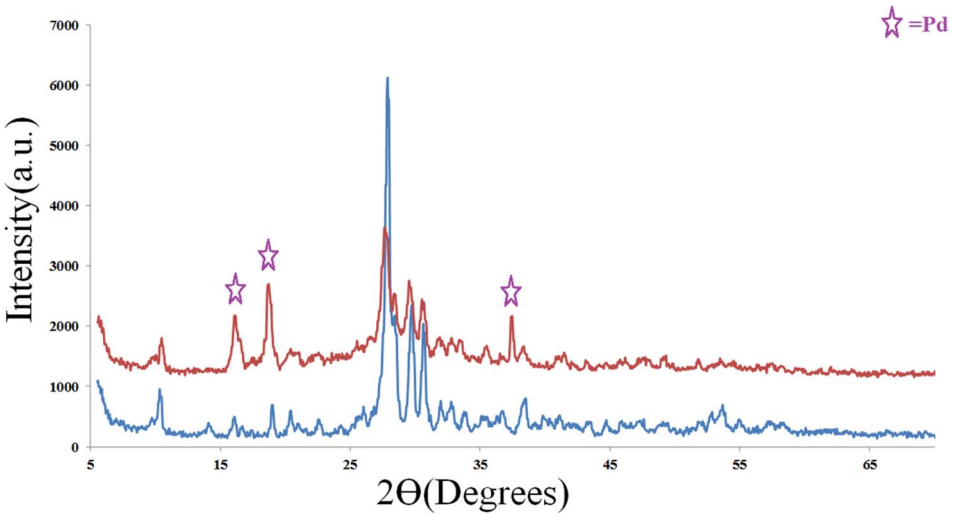

Fig. 5 X-ray diffraction (PXRD) for (blue) CON-KEY1 **5** and (red) Pd/CON-KEY1 **6**.

The EDX analysis of Pd/CON-KEY1 6 (Fig. 3) shows some signals related to the C, O, N, Cl, and Pd atoms in the structures, which agree with our predicted pattern of the synthesized structures. Regarding the palladium ions, the nanocatalyst showed that it contains 9.36% palladium ions in the ICP test report, which indicates good compatibility with the structure.[31,32]

The SEM photos of CON-KEY1 **5** and Pd/CON-KEY1 **6** (Fig. 4A and B) demonstrated the layered structures and morphology, indicating no specific changes after stabilizing palladium ions

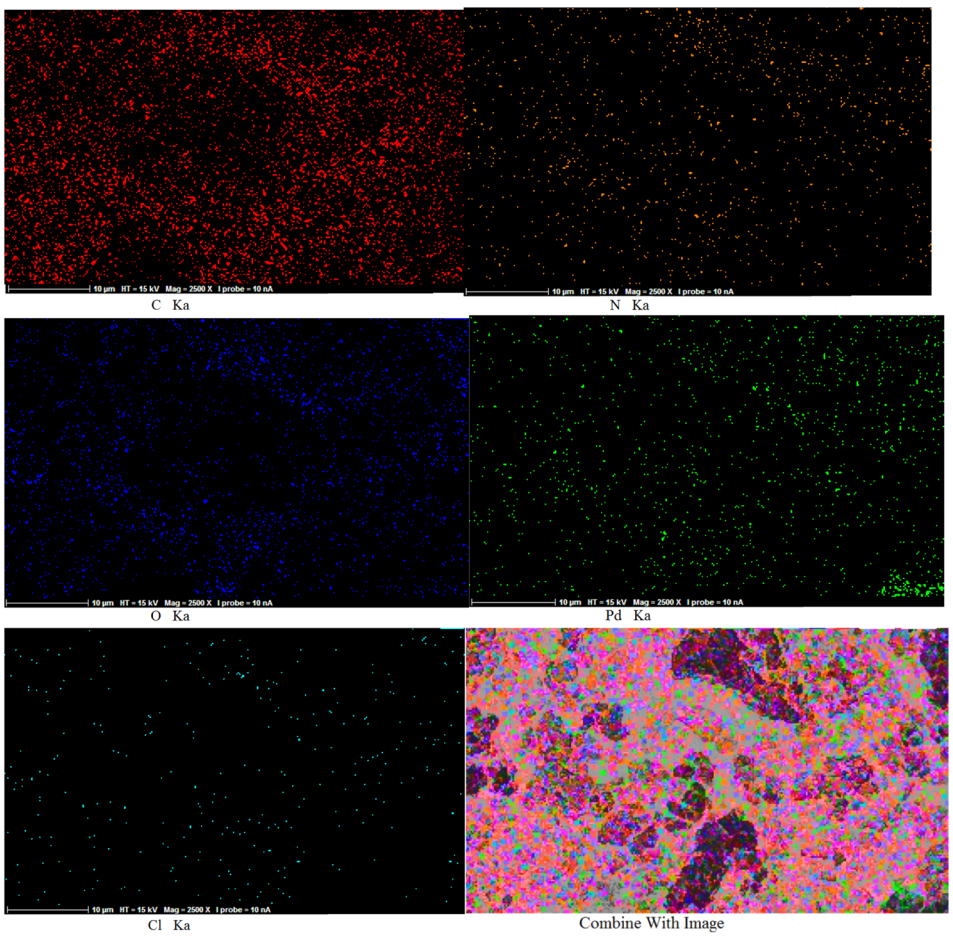

Fig. 6 X-ray mapping images of Pd/CON-KEY1 **6**.

on this nanocomposite. Fig. 4A and B shows the excellent dispersion of palladium ions in the CON-KEY1 **5** matrix. This nanocomposite must prevent the uniform accumulation of nanoparticles by trapping metal ions between the layers or inside its cavities.

SEM and TEM images of Pd/CON-KEY1 **6** (Fig. 4A–D) show the nature of the layered and porous structure of the catalytic nanocomposite. In the TEM images, the darker parts of the holes are due to the binding of palladium ions in the lattice structures of this nanocomposite.

As shown in the PXRD patterns (Fig. 5), the peak intensities of CON -KEY1 were decreased when $PdCl_2$ was embedded. Considering that COFs are composed of light elements, like C, H, N, *etc.*, the decreased intensities of the XRD peaks do not mean that the crystal structure of CON-KEY1 was destroyed after mixing with $PdCl_2$. Similar observations have been reported for other COFs caused by amorphous alkyl chains on the walls or guest molecules incorporated within the pores of the COFs. Some different new diffraction peaks appeared related to palladium chloride attached to the structure.

We applied elemental mapping to complete a study on the elemental composition and distribution of Pd/CON-KEY1 **6** (Fig. 6). Moreover, the elemental mapping results agree with the EDX patterns. The elemental map image shows a well-uniform

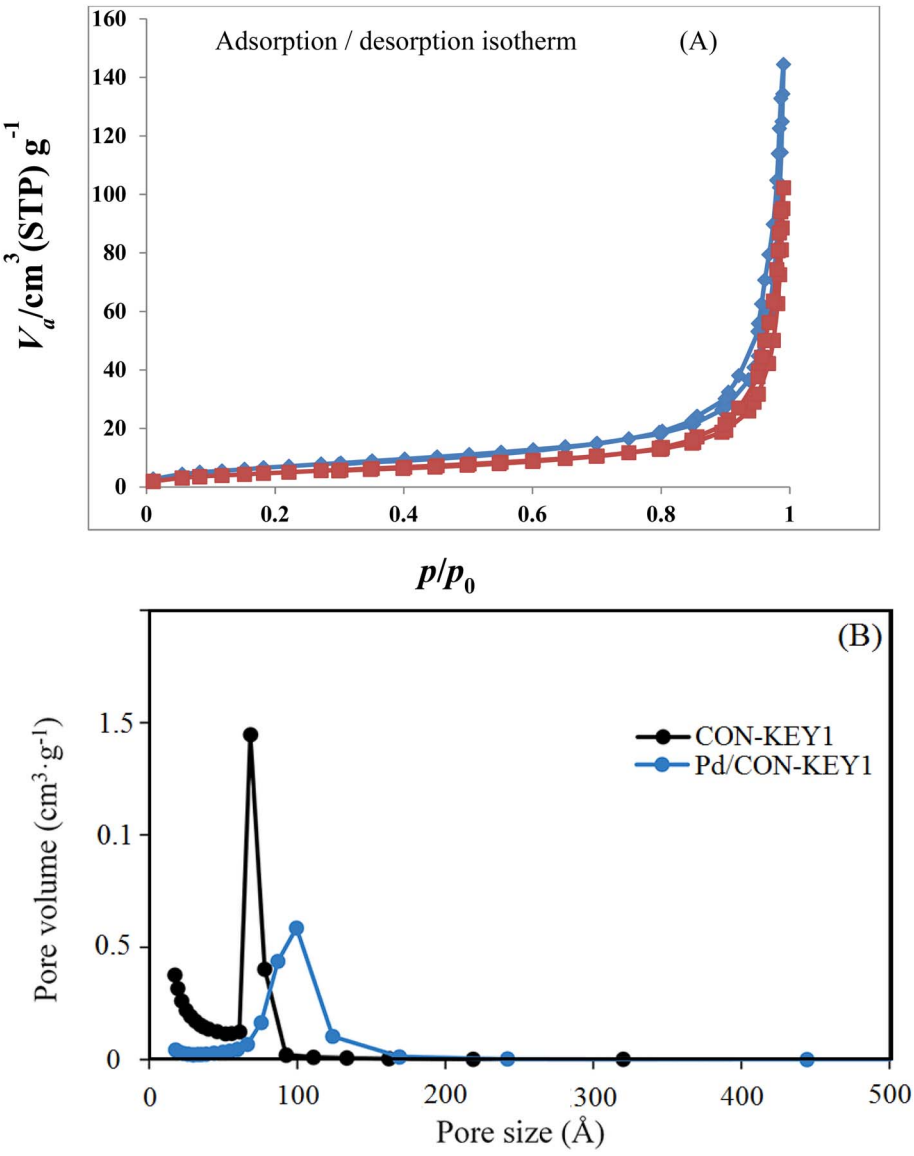

Sample	S_{BET} (m^2 g^{-1})	Total pure volume (cm^3 g^{-1})	Mean pore diameter (nm)
CON-KEY1 5	26.60	1.49	80.57
Pd/CON-KEY1 6	18.84	0.52	100.03

Fig. 7 N_2 adsorption–desorption isotherms (A) and the pore size distribution analysis based on the NLDFT model (B).

distribution of the exponential elements (N, O, C, Cl, and Pd) in the Pd/CON-KEY1 **6** catalyst, which confirms the heterogenized Pd/CON-KEY1 6 complex formation. Furthermore, the distribution of Pd elements reveals the coordination of the resulting framework to the amide groups and confirms the formation of the catalyst support. Moreover, the distribution of C, N, O, Cl, and Pd species indicates that the final metal catalyst is uniformly coordinated to the poly amide and nitrogen inside ring aromatic ligands, forming a Pd complex on the catalyst support.

The N_2 adsorption/desorption technique was used to determine surface structural parameters. The results of N_2 adsorption/desorption were plotted in Fig. 7. The obtained surface area based on BET isotherm is 26.60 $m^2\ g^{-1}$ for CON-KEY1 and 18.84 $m^2\ g^{-1}$ for Pd/CON-KEY1 **6**. The total pore volume of the composite polymer is 1.49 $cm^3\ g^{-1}$ for CON-KEY1 **5** and 0.52 $cm^3\ g^{-1}$ for Pd/CON-KEY1 **6**. Also, for studying the textural properties of Pd/CON-KEY1 **6**, the N_2 adsorption–desorption isotherms were used (Fig. 7). The adsorption isotherm is type III, and the appearance of hysteresis loop shows the presence of mesoporous in the sample. The pore size distribution of CON-KEY1 **5** and Pd/CON-KEY1 **6** based on the BJH method is shown.

3.1.1 Geometric shape optimization. Initial optimization was performed to guess the geometry of CON-KEY1 **5**. Then full optimizations were done for the repeat units of CON-KEY1 **5** and Pd/CON-KEY1 **6**. Two forms for Pd/CON-KEY1 **6** were considered: One is a form with Pd–N bonds, and the other consists of Pd–O bonds (Fig. 8). According to the equation $\Delta E_{binding} = [E_{complex} - (E_{CON\text{-}KEY1} + E_{PdCl_2})]$, the binding energies of the compounds were calculated in kcal mol^{-1} (Table 2). The results showed that the structure having Pd–N bonds in the bridge state is ~48 658 kcal mol^{-1} more stable than the one with Pd–O bonds, and the priority to form complex is the coordination of Pd to N atoms. Based on the bond angle results, in each structure, there are two positions in the layers for Pd to make a square planner complex with pyridine moieties of CON-KEY1 **5** in which their Pd–N and Pd–Cl bond lengths, as well as their bond angles, are almost the same. The bridge positions Pd–N and Pd–O bond lengths are 2.23 Å and 2.20–2.26 Å, respectively. In Pd–N/CON-KEY1 **6a**, the Pd–N distance in the layer (2.06 Å) is shorter than in the bridge position (2.23 Å). The same result happens for the Pd–Cl distances in both structures. Hence, the tetrahedral geometry in Pd–O/CON-KEY1 **6b** is slightly more distorted than Pd–N/CON-KEY1 **6a**.[33]

Table 2 Calculated $\Delta E_{binding}$ (kcal mol^{-1}), selected bond lengths (Å), bond angles (°), and global descriptors of Pd–N/CON-KEY1 **6a** and Pd–O/CON-KEY1 **6b**

System	Bond length/bond angles	Global descriptors	
Pd–N/CON-KEY1 **6a**	$Pd–N_{(bridge)}$ 2.23	E_{HOMO}	−0.030
	$Pd–Cl_{(bridge)}$ 2.51, 2.55	E_{LUMO}	0.0595
	$Pd–N_{(layer)}$ 2.06	E_g	0.089
	$Pd–Cl_{(layer)}$ 2.39–2.42	μ	0.015
	$N–Pd–N_{(bridge)}$ 98.7	η	0.045
$\Delta E_{binding} = -8220.05$	$Cl–Pd–Cl_{(bridge)}$ 110.0	S	22.35
	$Cl–Pd–N_{(bridge)}$ 102.0	ω	0.0025
	$N–Pd–N_{(layer)}$ 80.2		
	$Cl–Pd–Cl_{(layer)}$ 90.8		
	$Cl–Pd–N_{(layer)}$ 93.0		
Pd–O/CON-KEY1 **6b**	Pd–O 2.20, 2.26	E_{HOMO}	−0.241
	$Pd–Cl_{(bridge)}$ 2.39, 2.53	E_{LUMO}	−0.120
	$Pd–N_{(layer)}$ 2.06	E_g	0.12
	$Pd–Cl_{(layer)}$ 2.38–2.40	μ	−0.181
	O–Pd–O 85.6	η	0.061
$\Delta E_{binding} = 40\,438.18$	$Cl–Pd–Cl_{(bridge)}$ 107.0	S	16.53
	Cl–Pd–O 106.0	ω	0.269
	N–Pd–N 80.1		
	Cl–Pd–Cl 91.2		
	Cl–Pd–N 94.1		

In an attempt to find the reactivity and chemical potential of the systems, was done the NBO analysis. In addition, the energies of HOMO and LUMO frontier orbitals and the quantum molecular descriptors were calculated *via* Koopman's procedure.[34] In CON-KEY1 **5**, HOMO is located on the pyridine rings and C=O parts, while LUMO is on the other aromatic rings (Fig. 9). The energy gaps (E_g) between HOMO and LUMO are given in Table 2. The more decrease the E_g, the more facilitates the release of electrons from HOMO and the addition of electrons to LUMO, and the more reactive the compound. Other criteria for the reactivity or stability of a compound are μ (chemical potential) and η (hardness). Pd–N/CON-KEY1 **6a** has larger μ (0.015 eV) and smaller E_g (0.089 eV) and η (0.045 eV) compared to Pd–O/CON-KEY1 **6b**. So it is inferred that Pd–N/CON-KEY1 **6a** shows more reactivity and electron conductivity. Hence, charge transfer readily occurs within the system. Also, the softness (S) of Pd–N/CON-KEY1 **6a** is 22.35 eV which is high compared to Pd–O/CON-KEY1 **6b** (16.53 eV). So the former is more polarizable than the latter.[35] The systems electrophilicity index (ω) indicates the strong nucleophilic behavior of the Pd–N/CON-KEY1 **6a** contrasted with Pd–O/CON-KEY1 **6b**.

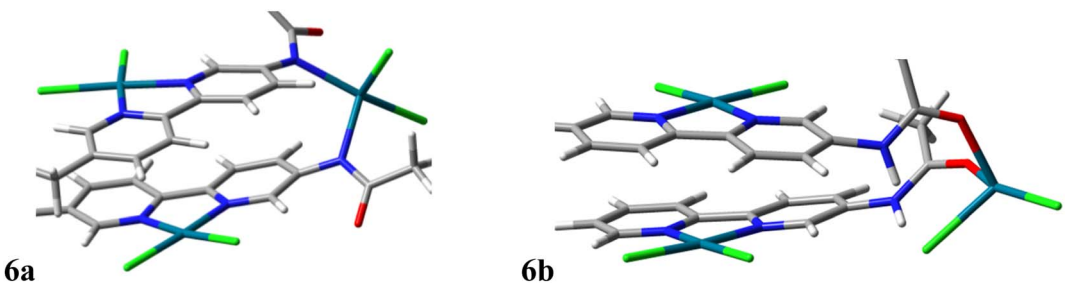

Fig. 8 The optimized structures of (a) Pd–N/CON-KEY1 **6a**, and (b) Pd–O/CON-KEY1 **6b** at B3LYP/lanl2dz level of theory.

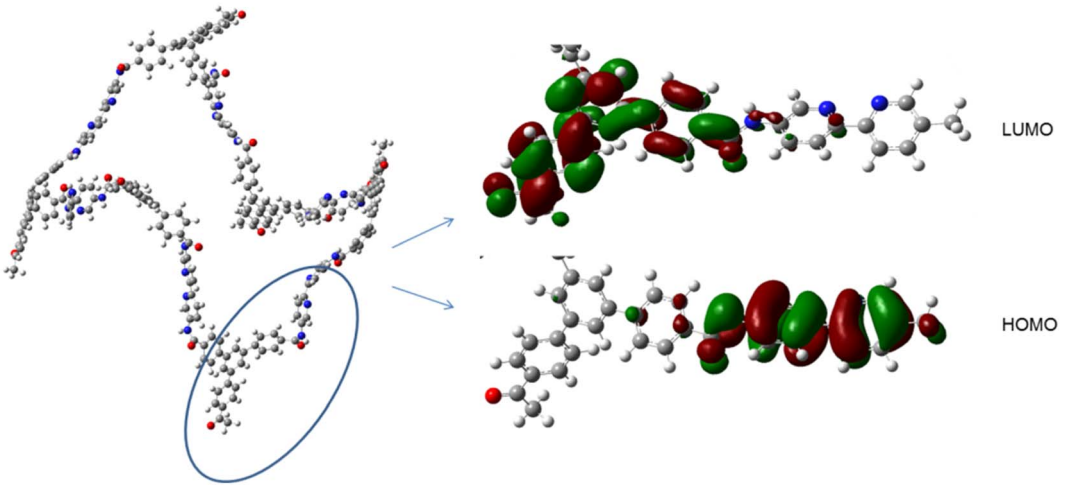

Fig. 9 The calculated HOMO and LUMO frontier orbitals of CON-KEY1 **5**.

3.2. Catalytic application of Pd/CON-KEY1 6

To optimize the parameters involved in the Mizoroki–Heck reaction, a model reaction was carried out with iodobenzene **7a** and styrene **8a**, and the results are shown in Table 3.

The results of the Heck cross-coupling reactions are shown in Scheme 3. The highly efficient substituted product *E* is readily obtained from various aryl iodides and Pd/CON-KEY1 **6** as a catalyst under standard Heck cross-coupling reaction conditions. High efficiency and spatial selectivity (*trans* products **9a–f**) are notable features of this reaction.

To optimize the parameters involved in the Suzuki–Miyaura coupling reaction, a model reaction was carried out with iodobenzene **7a** and phenyl boronic acid **10a**, and the results are shown in Table 4 (Table 4, entries 1–15).

Scheme 4 shows the catalytic role of Pd/CON-KEY1 **6** in the production of biaryl compounds **11a–l** under optimized reaction conditions. As expected, the aryl iodides afforded the desired biaryls with high reaction yields. For example, aryl iodide containing *m*-substituted NO_2 was converted to the desired *m*-nitro biphenyl yielding 94%. C–C coupling reaction yield of *p*-iodoanisole was 95%. For aryl iodide bearing *p*-Me,

Table 3 Optimization Screenings

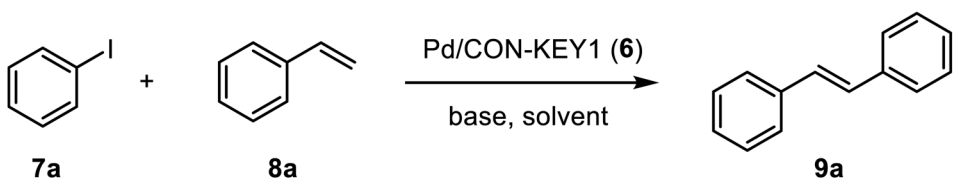

Entry	Catalyst 6 (mg)	Solvent	Base	*T* (°C)	Time (h)	Yield (%)
1	30	DMF	K_2CO_3	120	6	96
2	30	Toluene	K_2CO_3	120	6	69
3	30	DMSO	K_2CO_3	120	6	65
4	30	NMP	K_2CO_3	120	6	58
5	30	DMF	Na_2CO_3	120	6	86
6	30	DMF	KOH	120	6	46
7	30	DMF	NaOH	120	6	39
8	30	DMF	K_2CO_3	100	6	85
9	30	DMF	K_2CO_3	50	6	55
10	5	DMF	K_2CO_3	120	6	26
11	10	DMF	K_2CO_3	120	6	61
12	20	DMF	K_2CO_3	120	6	73
13	40	DMF	K_2CO_3	120	6	96
14	30	DMF	K_2CO_3	120	2	55
15	30	DMF	K_2CO_3	120	4	75
16	30	DMF	K_2CO_3	120	8	96

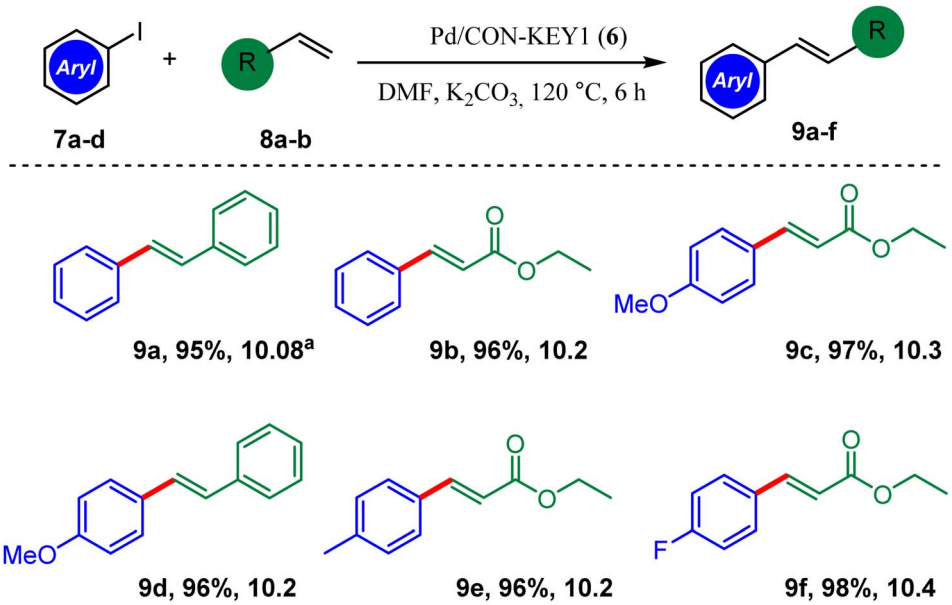

Scheme 3 Heck cross-coupling reactions of aryl iodide with acrylate derivatives and styrene. [a]TON = yield/amount of catalyst (mol).

Table 4 Optimization Screenings

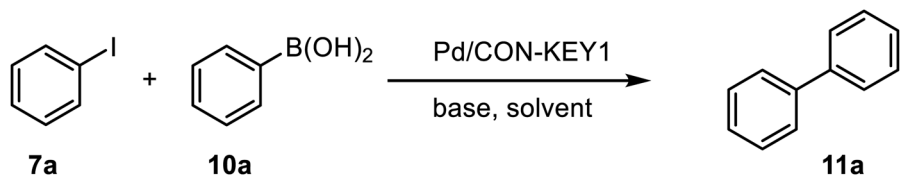

Entry	Catalyst **6** (mg)	Solvent	Base	*T* (°C)	Time (h)	Yield (%)
1	30	DMF	K_3PO_4	120	6	95
2	30	Toluene	K_3PO_4	120	6	60
3	30	DMSO	K_3PO_4	120	6	60
4	30	NMP	K_2CO_3	120	6	52
5	30	DMF	Na_2CO_3	120	6	76
6	30	DMF	KOH	120	6	44
7	30	DMF	NaOH	120	6	41
8	30	DMF	K_3PO_4	100	6	85
9	30	DMF	K_3PO_4	50	6	53
10	10	DMF	K_3PO_4	120	6	61
11	20	DMF	K_3PO_4	120	6	65
12	40	DMF	K_3PO_4	120	6	95
13	30	DMF	K_3PO_4	120	2	56
14	30	DMF	K_3PO_4	120	4	65
15	30	DMF	K_3PO_4	120	8	95

the yield was 86%. More importantly, it was observed that excellent product yields were attained when aryl bromides were used as an aryl halide source. 98% and 95% yields were observed in the C–C reaction of *p*-bromobenzonitrile and *p*-bromonitrobenzene, respectively. The desired biphenyl with a 93% yield was reached for *m*-bromonitrobenzene. Pd/CON KEY1 successfully catalyzed the C–C reaction of *p*-bromotoluene with a yield of 88%.

3.3. Comparison activity of Pd/CON-KEY1 with other catalysts

The advantages of the produced nanocatalyst are summarized in Tables 5 and 6, in which its properties are compared with various catalytic systems. Accordingly, the catalytic system presented in this study offers higher efficiency than other systems for this reaction regarding the reaction yield and time.

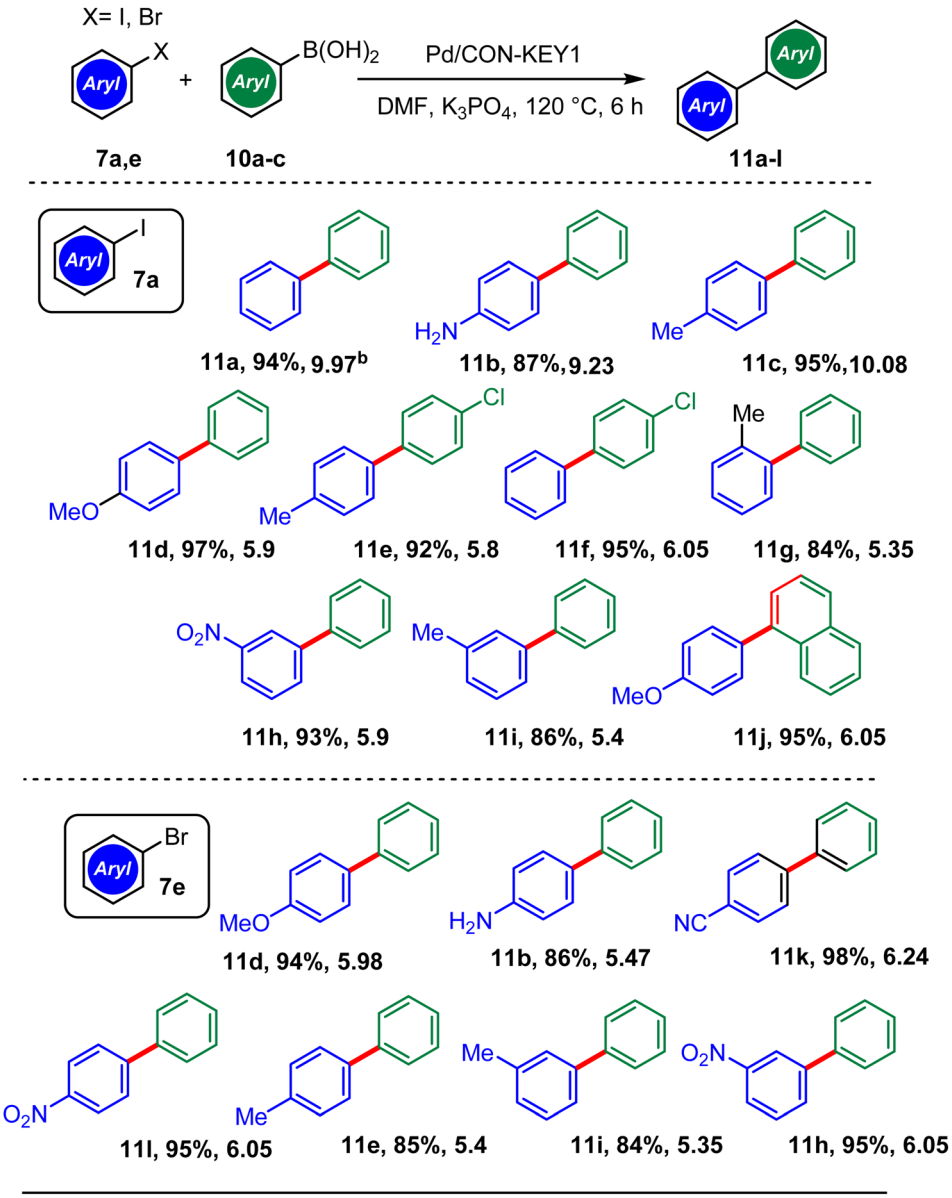

Scheme 4 Pd/CON-KEY1 catalyzed Suzuki–Miyaura coupling reaction.[a] [a]Reaction conditions: Ar-X **7** (0.5 mmol), $ArB(OH)_2$ **10** (0.6 mmol), K_3PO_4 (0.6 mmol) and Pd/CON-KEY1 **6** catalyst (30 mg). [b]TON = yield/amount of catalyst (mol).

Table 5 Comparison of the activity of some catalysts with Pd/CON-KEY1 **6** for the Suzuki–Miyaura reaction among phenyl iodide and benzene boronic acid

Entry	Catalyst	Conditions	Time (h)	Yield (%)	Ref.
1	Pd imino-Py-γ-Fe_2O_3	Et_3N, DMF, 100 °C	0.5	95	36
2	γ-Fe_2O_3-acetamidine-Pd	Et_3N, DMF, 100 °C	0.5	96	37
3	Pd-Py-MCM-41	Na_2CO_3, PEG, 80 °C	2	97	38
4	LDH-Pd(0)	K_2CO_3, 1,4-dioxane-H_2O, 80 °C	10	96	39
5	MCM-41-S-Pd(0)	K_2CO_3, DMF-H_2O, 80 °C	6	98	40
6	Pd-BIP-γ-Fe_2O_3@SiO_2	Et_3N, DMF, 100 °C	1	98	41
7	Fe_3O_4-Bpy-Pd$(OAc)_2$	K_2CO_3, toluene, 80 °C	6	99	42
8	Fe_3O_4@SiO_2@*m*SiO_2-Pd(II)	K_2CO_3, EtOH, 80 °C	3	98	43
9	Pd(II)–NHC complex	Cs_2CO_3, DMF, 100 °C	24	99	44
10	Pd/CON-KEY1 **6**	K_3PO_4, DMF, 120 °C	6	97	This work

Table 6 Comparison of the activity of some catalysts with Pd/CON-KEY1 for the Heck cross-coupling between phenyl iodide and ethyl acrylate

Entry	Catalyst	Conditions	Time (h)	Yield (%)	Ref.
1	Fe_3O_4@SiO_2/Schiff base/Pd(II)	K_2CO_3, DMF, 110 °C	0.75	97	45
2	Pd-NPs	Et_3N, IL, 100 °C	3	87	46
3	Pd/Fe_3O_4	K_2CO_3, NMP, 130 °C	5	99	47
4	Pd/6c complex	K_2CO_3, DMAc, 120 °C	2	97	48
5	Fe_3O_4/DAG/Pd	Et_3N, DMF, 110 °C	0.5	96	49
6	NHC–Pd(II)	Na_2CO_3, DMA, 160 °C	18	99	50
7	$Pd(OAc)_2$@MNP	Et_3N, DMF, 100 °C	1	97	51
8	Pd-isatin Schiff base-γ-Fe_2O_3	Et_3N, solvent-free, 100 °C	0.5	95	52
9	SiO_2@Fe_3O_4–Pd	K_2CO_3, DMF, 100 °C	8	97	53
10	Pd/CON-KEY1 **6**	K_2CO_3, DMF, 120 °C	2–6	98	This work

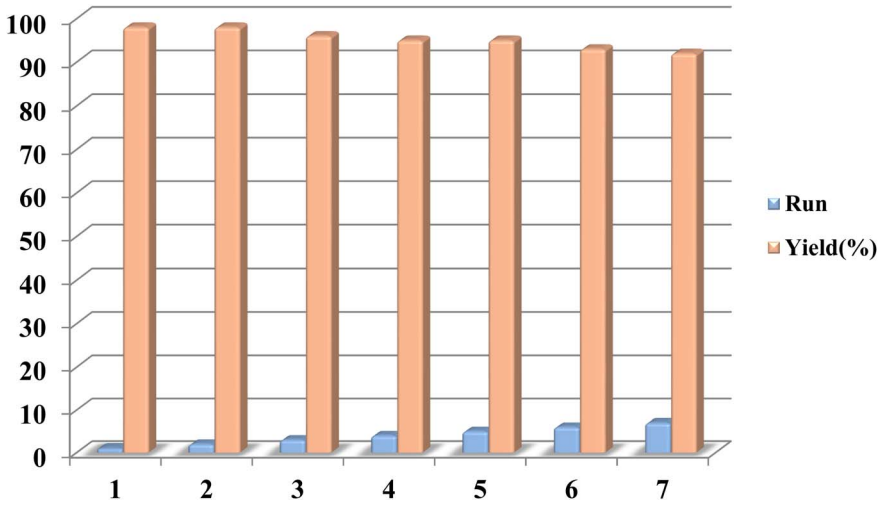

Fig. 10 Recycling experiment of the Pd/CON-KEY1 **6** for the reaction of phenyl iodide and ethyl acrylate.

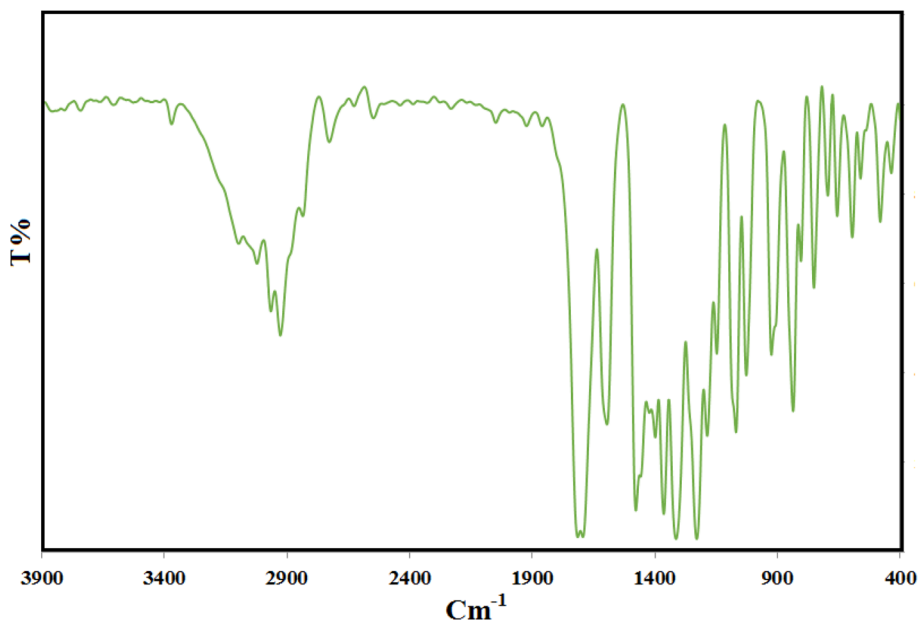

Fig. 11 FT-IR spectrum for Pd/CON-KEY1 **6** catalyst after recovery.

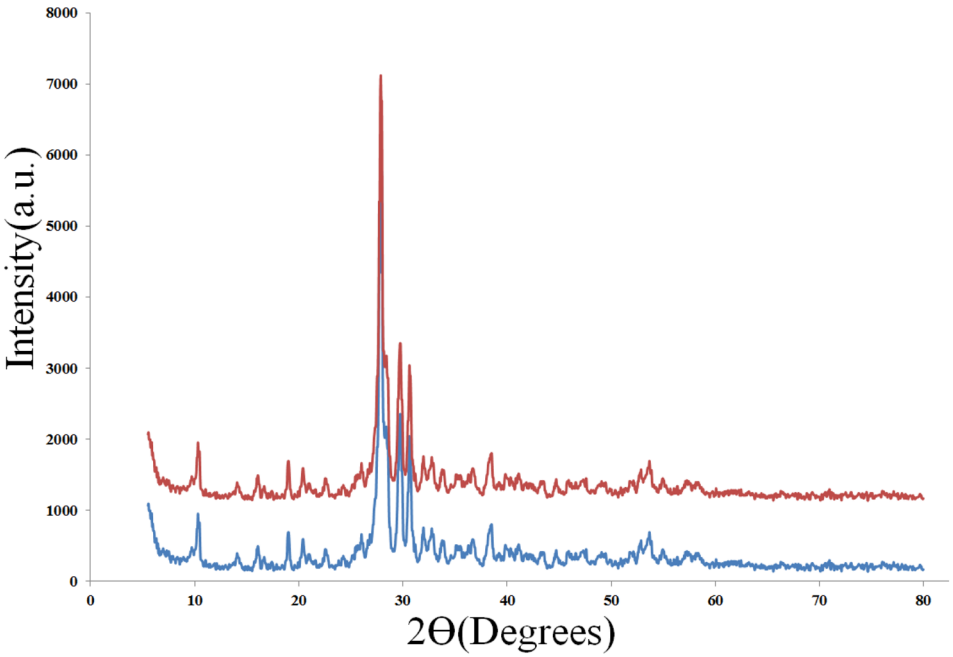

Fig. 12 X-ray diffraction (PXRD) of (blue) fresh and (red) reused Pd/CON-KEY1 **6** catalyst after recovery.

The advantages of Pd/CON-KEY1 **6** as the catalyst include having a higher yield, a less intensive process, and easier separability and recyclability several times (entry 10).

3.4. Reusability of Pd/CON-KEY1 6 nanocatalyst

Finally, it is worth mentioning that recycling and reusing the catalysts have become a prospect for the synthesis of longer-lasting catalysts due to their high manufacturing costs and environmental conditions. Once the reaction is completed, the Pd/CON-KEY1 **6** catalyst can be easily separated from the reaction mixture *via* filtration and reused in subsequent reactions after being washed with water and ethanol and dried in a vacuum. Significantly, more than an average of 98% of catalysts can be recovered each time (Fig. 10).

This study's Pd/CON-KEY1 **6** catalyst recovery indicates a high-efficiency sequential application. A survey of the FT-IR spectrum(Fig. 11) & X-ray diffraction (PXRD) (Fig. 12) for the Pd/CON-KEY1 **6** catalyst after recovery of the synthesized nanocatalyst shows the stability of this catalyst.

After theoretical and experimental studies on these modified nano polymers and proving their stability in reactions, it is necessary to use this class of compounds more than before.

4. Conclusion

Here we reported the facile synthesis of a novel amide-based CON through the reaction of CDI, [2,2′-bipyridine]-5,5′-diamine(BDA) and 1,3,5-tris(4-carboxyphenyl)benzene (TCB). Loading the obtained CON(CON-KEY1) with palladium chloride resulted in an efficient catalyst for Suzuki and Heck coupling reactions. The CON-Pd/CON-KEY1 catalyst was characterized by ICP-OES, TG-DTA, FT-IR, EDX, XRD, TEM, XPS, Element mapping and N_2 isotherms. Theoretical studies proved the formation of the catalyst in an eclipsed-layered structure. This product was a heterogeneous active catalyst for Heck and Suzuki reactions. Other contributors are the cooperative effect between the amide sites and the large surface area and high porosity of CON. In addition, Pd/CON-KEY1 catalyst was found to be a multifunctional CON with robustness and stability under reaction conditions. Accordingly, it can be reused up to eight times without losing its catalytic activity and structural integrity. The other benefits of the proposed mesoporous catalyst include high yield, facile separation of the catalyst from the mixture, great TOF, and a clean reaction profile. This research portrays a bright future in using porous CONs and their functionalized analogs as multifunctional catalysts.

Conflicts of interest

The authors declare that they have no competing interests.

Acknowledgements

Any funding source had no role in the design of this study and will not have any role during its execution, analyses, interpretation of the data, or decision to submit results. The authors express appreciation to the Bu-Ali Sina University for supporting this investigation.

References

1 H. Keypour, *et al.*, Facile synthesis of a new covalent organic framework (COF-AYLIN) based on polyamide links and their application in CN coupling reaction, *Inorg. Chim. Acta*, 2023, **552**, 121494.

2 J. Kouhdareh, *et al.*, Pd (II)-immobilized on a novel covalent imine framework (COF-BASU1) as an efficient catalyst for asymmetric Suzuki coupling, *J. Mol. Struct.*, 2023, **1273**, 134286.
3 K. T. Tan, *et al.*, Covalent organic frameworks, *Nat. Rev. Methods Primers*, 2023, **3**(1), 1–19.
4 X. Feng, X. Ding and D. Jiang, Covalent organic frameworks, *Chem. Soc. Rev.*, 2012, **41**(18), 6010–6022.
5 R. K. Sharma, *et al.*, Recent development of covalent organic frameworks (COFs): synthesis and catalytic (organic-electro-photo) applications, *Mater. Horiz.*, 2020, **7**(2), 411–454.
6 K. Geng, *et al.*, Covalent organic frameworks: design, synthesis, and functions, *Chem. Rev.*, 2020, **120**(16), 8814–8933.
7 H. R. Abuzeid, A. F. EL-Mahdy and S.-W. Kuo, Covalent organic frameworks: Design principles, synthetic strategies, and diverse applications, *Giant*, 2021, **6**, 100054.
8 W. Zhang, *et al.*, Reconstructed covalent organic frameworks, *Nature*, 2022, **604**(7904), 72–79.
9 D. Ma, *et al.*, Covalent organic frameworks: promising materials as heterogeneous catalysts for CC bond formations, *Catalysts*, 2018, **8**(9), 404.
10 S.-Y. Ding, *et al.*, Construction of covalent organic framework for catalysis: Pd/COF-LZU1 in Suzuki–Miyaura coupling reaction, *J. Am. Chem. Soc.*, 2011, **133**(49), 19816–19822.
11 J. Liu, N. Wang and L. Ma, Recent advances in covalent organic frameworks for catalysis, *Chem. – Asian J.*, 2020, **15**(3), 338–351.
12 V. Sharma, M. Nemiwal and D. Kumar, Catalytic applications of recent and improved covalent organic frameworks, *Mini-Rev. Org. Chem.*, 2022, **19**(7), 815–825.
13 J. Kouhdareh, *et al.*, Immobilization of Ag and Pd over a novel amide based covalent organic framework (COF-BASU2) as a heterogeneous reusable catalyst to reduce nitroarenes, *Inorg. Chim. Acta*, 2023, **545**, 121251.
14 Y. Zhi, *et al.*, Recent progress in metal-free covalent organic frameworks as heterogeneous catalysts, *Small*, 2020, **16**(24), 2001070.
15 R. Karimi-Nami, *et al.*, Pd Immobilization Phenanthroline-2, 9-Dicarbaldehyde Modified Magnetic CuBDC MOF as a Reusable Heterogeneous Catalyst for Suzuki-Miyaura Cross-Coupling Reactions, *Polycyclic Aromat. Compd.*, 2023, 1–16.
16 M. Aghayee, *et al.*, Synthesis and characterization of a novel magnetic nano-palladium Schiff base complex: application in cross-coupling reactions, *Appl. Organomet. Chem.*, 2016, **30**(8), 612–618.
17 H. Keypour, *et al.*, Synthesis of magnetically recyclable Fe3O4@[(EtO) 3Si–L1H]/Pd (II) nanocatalyst and application in Suzuki and Heck coupling reactions, *Appl. Organomet. Chem.*, 2017, **31**(2), e3558.
18 M. Balali, *et al.*, Palladium Supported on Schiff Base Functionalized Magnetite Nanoparticles as an Efficient Catalyst for Coupling Reactions, *Inorg. Chem. Res.*, 2021, **5**(1), 82–93.
19 H. K. Jamal Kouhdareh and S. Alavinia, Anchorage of pd into modified isoreticular metal–organic framework-3 as a heterogeneous catalyst for mizoroki–heck cross-coupling reactions, *Acta Chem. Malays.*, 2022, **6**(1), 35–42.
20 J. K. Hassan Keypour, S. Alavinia and M. Taher Rezaei, Synthesis of magnetic nano catalyst using dopamine functionalized magnetic nano particles and investigation of its properties in mizoroki–heck cross-coupling reactions, *Acta Chem. Malays.*, 2023, **7**(1), 16–22.
21 R. Karimi-Nami, *et al.*, Pd Immobilization Phenanthroline-2, 9-Dicarbaldehyde Modified Magnetic CuBDC MOF as a Reusable Heterogeneous Catalyst for Suzuki-Miyaura Cross-Coupling Reactions, *Polycyclic Aromat. Compd.*, 2023, 1–16.
22 B. Agrahari, *et al.*, Synthesis, crystal structures, and application of two new pincer type palladium (II)-Schiff base complexes in CC cross-coupling reactions, *Inorg. Chim. Acta*, 2018, **471**, 345–354.
23 S. A. Jasim, *et al.*, Nanomagnetic Salamo-based-Pd (0) Complex: an efficient heterogeneous catalyst for Suzuki–Miyaura and Heck cross-coupling reactions in aqueous medium, *J. Mol. Struct.*, 2022, **1261**, 132930.
24 Y. Thopate, *et al.*, Cascade Multicomponent Reaction Involving Unprecedented Gould Jacobs–Heck/Suzuki Coupling-Hydrolysis-Decarboxylation Reactions in One Pot: Rapid Synthesis of Hybrid Heterocyclic Molecules, *Asian J. Org. Chem.*, 2022, **11**(8), e202200343.
25 R.-X. Liang and Y.-X. Jia, Aromatic π-components for enantioselective Heck reactions and Heck/anion-capture domino sequences, *Acc. Chem. Res.*, 2022, **55**(5), 734–745.
26 J. Kouhdareh, *et al.*, Immobilization of Ag and Pd over a novel amide based covalent organic framework (COF-BASU2) as a heterogeneous reusable catalyst to reduce nitroarenes, *Inorg. Chim. Acta*, 2022, 121251.
27 Z. Mohammadkhani, *et al.*, Synthesizing and post-synthetically modifying metal-organic frameworks (Co (BDC)-NH2) for carbonylative sonogashira coupling reaction, *J. Organomet. Chem.*, 2023, **999**, 122822.
28 H. Keypour, *et al.*, Stabilization of Au-Nanoparticle-Decorated Postsynthesis-Modified Cu (BDC-NH2) MOF as a Reusable Heterogeneous Catalyst in an Intermolecular Hydroamination of Allenamides with Arylamines, *J. Organomet. Chem.*, 2023, 122873.
29 H. Keypour, *et al.*, An Efficient Method for Enhancement in the catalytic activity of Dual-Porous Co (BDC-NH2) MOF Au-Decorated Nanoparticle through Post-Synthetic Modification, *J. Organomet. Chem.*, 2023, 122778.
30 H. Keypour, *et al.*, Development of sustainable green catalysts for oxidation of alcohols via decorated palladium nanoparticles on magnetic carbon nanotube/MOF, *J. Mol. Struct.*, 2023, **1294**, 136444.
31 J. Kouhdareh, *et al.*, Synthesis of a Au/Au NPs-PPy/l-CYs/ZIF-8 nanocomposite electrode for voltammetric determination of insulin in human blood, *RSC Adv.*, 2023, **13**(35), 24474–24486.
32 H. Keypour, *et al.*, Pd-Coordinated Salinidol-Modified Mixed MOF: An Excellent Active Center for Efficient Nitroarenes

Reduction and Selective Oxidation of Alcohols, *ACS Omega*, 2023, **8**(24), 22138–22149.

33 Z. Shariatinia and M. Abdollahi-Moghadam, DFT computations on surface physical adsorption of hydrocarbons produced in the Fischer-Tropsch synthesis on a CNT/Co nanocatalyst, *J. Saudi Chem. Soc.*, 2018, **22**(7), 786–808.

34 R. Hussain, *et al.*, Density functional theory study of palladium cluster adsorption on a graphene support, *RSC Adv.*, 2020, **10**(35), 20595–20607.

35 M. Abdollahi-Moghadam, *et al.*, An experimental and theoretical study of a new sensitive and selective Al3+ Schiff base fluorescent chemosensor bearing a homopiperazine moiety, *J. Mol. Struct.*, 2023, **1273**, 134289.

36 Y. Leng, *et al.*, Generally applicable and efficient oxidative Heck reaction of arylboronic acids with olefins catalyzed by cyclopalladated ferrocenylimine under base-and ligand-free conditions, *Tetrahedron*, 2010, **66**(6), 1244–1248.

37 L. Wang, H. Li and P. Li, Task-specific ionic liquid as base, ligand and reaction medium for the palladium-catalyzed Heck reaction, *Tetrahedron*, 2009, **65**(1), 364–368.

38 S. Sobhani, *et al.*, Palladium-Schiff base complex immobilized covalently on magnetic nanoparticles as an efficient and recyclable catalyst for Heck and Suzuki cross-coupling reactions, *Catal. Lett.*, 2016, **146**(1), 255–268.

39 S. Sobhani, *et al.*, Acetamidine–palladium complex immobilized on γ-Fe_2O_3 nanoparticles: a novel magnetically separable catalyst for Heck and Suzuki coupling reactions, *RSC Adv.*, 2014, **4**(83), 44166–44174.

40 M. Nikoorazm, A. Ghorbani-Choghamarani and A. Jabbari, A facile preparation of palladium Schiff base complex supported into MCM-41 mesoporous and its catalytic application in Suzuki and Heck reactions, *J. Porous Mater.*, 2016, **23**(4), 967–975.

41 S. Singha, M. Sahoo and K. Parida, Highly active Pd nanoparticles dispersed on amine functionalized layered double hydroxide for Suzuki coupling reaction, *Dalton Trans.*, 2011, **40**(27), 7130–7132.

42 L. Zhou, *et al.*, Recent advances in non-metal modification of graphitic carbon nitride for photocatalysis: a historic review, *Catal. Sci. Technol.*, 2016, **6**(19), 7002–7023.

43 S. Sobhani, Z. Zeraatkar and F. Zarifi, Pd complex of an NNN pincer ligand supported on γ-Fe2O3@ SiO2 magnetic nanoparticles: a new catalyst for Heck, Suzuki and Sonogashira coupling reactions, *New J. Chem.*, 2015, **39**(9), 7076–7085.

44 Y.-Q. Zhang, X.-W. Wei and R. Yu, Fe_3O_4 nanoparticles-supported palladium-bipyridine complex: effective catalyst for Suzuki coupling reaction, *Catal. Lett.*, 2010, **135**(3), 256–262.

45 M. Nasrollahzadeh, S. M. Sajadi and M. Maham, Green synthesis of palladium nanoparticles using Hippophae rhamnoides Linn leaf extract and their catalytic activity for the Suzuki–Miyaura coupling in water, *J. Mol. Catal. A: Chem.*, 2015, **396**, 297–303.

46 Q. Xu, *et al.*, A novel cis-chelated Pd (II)–NHC complex for catalyzing Suzuki and Heck-type cross-coupling reactions, *Tetrahedron*, 2005, **61**(47), 11225–11229.

47 M. Esmaeilpour and J. Javidi, Magnetically-recoverable Schiff Base Complex of Pd (II) Immobilized on Fe3O4@ SiO2 Nanoparticles: An Efficient Catalyst for Mizoroki–Heck and Suzuki–Miyaura Coupling Reactions, *J. Chin. Chem. Soc.*, 2015, **62**(7), 614–626.

48 D. S. Gaikwad, Y. Park and D. M. Pore, A novel hydrophobic fluorous ionic liquid for ligand-free Mizoroki–Heck reaction, *Tetrahedron Lett.*, 2012, **53**(24), 3077–3081.

49 X. Liu, *et al.*, 2D phosphorene nanosheets, quantum dots, nanoribbons: synthesis and biomedical applications, *Biomater. Sci.*, 2021, **9**, 2768–2803.

50 A.-E. Wang, *et al.*, Triaryl phosphine-functionalized N-heterocyclic carbene ligands for Heck reaction, *Tetrahedron*, 2005, **61**(1), 259–266.

51 H. Veisi, A. Sedrpoushan and S. Hemmati, Palladium supported on diaminoglyoxime-functionalized Fe3O4 nanoparticles as a magnetically separable nanocatalyst in Heck coupling reaction, *Appl. Organomet. Chem.*, 2015, **29**(12), 825–828.

52 T. Chen, J. Gao and M. Shi, A novel tridentate NHC–Pd (II) complex and its application in the Suzuki and Heck-type cross-coupling reactions, *Tetrahedron*, 2006, **62**(26), 6289–6294.

53 Q. Zhang, *et al.*, Covalently anchored tertiary amine functionalized ionic liquid on silica coated nano-Fe3O4 as a novel, efficient and magnetically recoverable catalyst for the unsymmetrical Hantzsch reaction and Knoevenagel condensation, *RSC Adv.*, 2017, **7**(85), 53861–53870.